Atmos. Chem. Phys. Discuss., 8, 12227–12252, 2008
www.atmos-chem-phys-discuss.net/8/12227/2008/
© Author(s) 2008. This work is distributed under
the Creative Commons Attribution 3.0 License.

Atmospheric Chemistry and Physics Discussions

Middle atmospheric water vapour and dynamics in the vicinity of the polar vortex during the Hygrosonde-2 campaign

S. Lossow[1], M. Khaplanov[1], J. Gumbel[1], J. Stegman[1], G. Witt[1], P. Dalin[2], S. Kirkwood[2], J. D. Schmidlin[3], K. H. Fricke[4], and A. Blum[4]

[1]Department of Meteorology, Stockholm University, 10691 Stockholm, Sweden
[2]Swedish Institute of Space Physics, 98128 Kiruna, Sweden
[3]NASA Goddard Space Flight Center, Wallops Island, VA 23681, USA
[4]Physikalisches Institut der Universität Bonn, 53115 Bonn, Germany

Received: 22 April 2008 – Accepted: 23 May 2008 – Published: 20 June 2008

Correspondence to: S. Lossow (stefan.lossow@misu.su.se)

Published by Copernicus Publications on behalf of the European Geosciences Union.

Abstract

The Hygrosonde-2 campaign took place on 16 December 2001 at Esrange/Sweden, with the aim to investigate the small scale distribution of water vapour in the middle atmosphere in the vicinity of the Arctic polar vortex. In-situ balloon and rocket-borne measurements of water vapour were performed by means of OH fluorescence hygrometry. The combined measurements yielded a high resolution water vapour profile up to an altitude of 75 km. Using water vapour as a dynamical tracer it was possible to directly relate the water data to the position of the polar vortex. The measurement probed extra-vortex air below 19 km and in the altitude range between 45 km and 60 km and vortex air elsewhere. Transitions between vortex and extra-vortex usually coincided with wind shears caused by gravity waves which advect air masses with different water vapour characteristics. From the combination of the results from the Hygrosonde-2 campaign and the first flight of the optical hygrometer in 1994 (Hygrosonde-1) a clear picture of the characteristic water vapour distribution inside and outside the polar vortex can be drawn. Systematic differences in the water vapour concentration between the inside and outside of the polar vortex can be observed all the way up into the mesosphere and are consistent with efficient downward transport of air inside the vortex. It is evident that in-situ measurements with high spatial resolution are needed to fully account for the small-scale exchange processes in the polar winter middle atmosphere.

1 Introduction

Water vapour plays a major role in the radiative budget and chemistry of the Earth's atmosphere. Recent research on middle atmospheric water vapour has focused on global trends in the stratosphere (e.g. Oltmans et al., 2000; Michelsen et al., 2000; Rosenlof et al., 2001; Nedoluha et al., 2003; Randel et al., 2004) and their impacts on the ozone destruction by polar stratospheric clouds (PSC) in the polar vortex (e.g. Rex et al., 2004), troposphere-stratosphere exchange (e.g. SPARC, 2000; Sherwood and

ACPD

8, 12227–12252, 2008

Dessler, 2000; Bonazzola and Haynes, 2004; Engel et al., 2006; Lelieveld et al., 2006), and the water budget in the summer mesopause region (e.g. von Zahn and Berger, 2003).

Water vapour enters the middle atmosphere mostly by vertical transport trough the tropical tropopause transition layer (TTL). The tropical tropopause works as a cold trap where freeze-drying of water vapour and subsequent sedimentation of ice particles strongly reduces the amount of water vapour entering the stratosphere (Brewer, 1949). The water throughput at the tropical tropopause is about 3.7 ppmv (e.g. SPARC, 2000; Nassar et al., 2005) and has a seasonal variation that is governed by the tropopause temperature. The observed temporal evolution is usually referred to as the tape recorder effect (Mote et al., 1996). Besides the transport from the troposphere the only water vapour source in the stratosphere is oxidation of methane. Sink processes like photodissociation and the reaction with $O(^1D)$ do not become relevant below the mesosphere which consequently leads to an increase of the water vapour concentration with altitude throughout the stratosphere. The balance between these source and sink processes is usually observed around the stratopause resulting in a maximum in the water vapour concentration ("conventional maximum"). Above in the mesosphere, the concentration of water vapour decreases in general with altitude due to the lack of additional sources. There are two pronounced exceptions from this general mesospheric behaviour, which can only occur limited in space and time. The first one is an additional peak between 65 km and 75 km occuring both in the tropics around equinox and in the polar region in summer (Nedoluha et al., 1996; Summers et al., 1997; Seele and Hartogh, 1999). This peak is produced by an interplay between dynamics and chemistry during strongest solar insolation, involving upwelling winds and autocatalytical water vapour formation from the molecular hydrogen reservoir (Sonnemann et al., 2005). The second peak can be observed around 82 km in the polar summer and is due to water vapour redistribution by sedimenting ice particles forming noctilucent clouds (NLC) and polar mesospheric summer echoes (PMSE) (Summers et al., 2001; von Zahn and Berger, 2003).

ACPD
8, 12227–12252, 2008

The chemical and vertical transport life time of water vapour in the middle atmosphere are comparable, i.e. in the order of months. Hence, in the absence of condensation, water vapour is particularly suitable as a tracer of dynamical processes (Brasseur and Solomon, 1994). One typical application is the polar vortex. The wave driven meridional circulation gives rise to large scale subsidence of air inside the polar vortex. In addition the polar vortex edge efficiently prevents horizontal transport of chemical species from the mid-latitudes. Both aspects result in significant horizontal contrasts and gradients in the water vapour concentration across the polar vortex edge. At an altitude level in the lower and middle stratosphere the water vapour concentration will be in general higher inside the vortex than outside due to the subsidence of moister air from higher stratospheric levels inside the vortex. This excludes possible dehydration effects due to polar stratospheric clouds type II (composed of water ice) (Kelly et al.,1989; Vömel et al., 1995). The influence of the polar vortex on the water vapour distribution extends well into the mesosphere (Aellig et al., 1996). More recent satellite measurements by the Fourier Transform Spectrometer (FTS) instrument onboard the Canadian ACE/SCISAT-1 satellite (Bernath et al., 2005) observed differences in the water vapour characteristics inside and outside the polar vortex as high as in 77 km (Nassar et al., 2005). At mesospheric altitudes the water vapour concentration will be in general lower inside the polar vortex than outside polar vortex due to the subsidence of drier air masses from above inside the polar vortex.

The polar vortex border is not just a well-defined discontinuity, but tends to exhibit filamentation and layering. This is caused by irreversible planetary wave breaking at the vortex edge and can be seen as lamination in tracer profiles (Reid and Vaughan, 1991). These filaments are stretched by the polar jet and will be gradually dissipated or mixed with mid-latitude air. At the polar vortex edge also gravity waves can lead to lamination structures in the water vapour profile. These waves can, in general, only influence the water vapour concentration in regions where the concentration exhibits strong vertical or horizontal gradients due to the advection of air masses with different characteristics.

ACPD
8, 12227–12252, 2008

In order to resolve such small scale dynamical structures, as observed in the vicinity of the polar vortex edge, high resolution in-situ measurements are necessary. These measurements are an important complement to ground-based and satellite-borne measurements as well for the evaluation of models. The vertical resolution of ground-based radiometer measurements is not sufficient enough to resolve small scale structures. In order to increase the signal-to-noise ratio these measurements usually need to be integrated over a longer period of time during which small scale structures could have changed already. Satellite data represent a mean over a horizontal path of several hundred kilometres at the single tangent heights. This makes it very difficult to analyse local structures, especially when there are strong horizontal gradients present as at the edge of the polar vortex. Also results from the ECMWF (European Centre for Medium-range Weather Forecast) model do not characterise satisfactorily the water vapour distribution in the polar vortex edge region in the lower and middle stratosphere (Maturilli et al., 2006). High resolution in-situ measurements of water vapour are well established in the lower and middle stratosphere. Higher up, in the upper stratosphere and mesosphere, such kind of measurements are extremely rare. In this paper we present a high resolution water vapour measurement from the Hygrosonde-2 campaign in the vicinity of the polar vortex, covering the middle atmosphere up to an altitude of 75 km. This campaign is a continuation of the measurements performed during the Hygrosonde-1 campaign in 1994 (Khaplanov et al., 1996). In next section (Sect. 2) we give an overview of the observations. We describe the results in Sect. 3. The subsequent discussion in Sect. 4 also includes the results from Hygrosonde-1, with focus on water vapour as a dynamical tracer.

2 Experiments

The Hygrosonde-2 campaign comprised a comprehensive set of experiments to measure the middle atmospheric water vapour concentration and the background state of the atmosphere. The high resolution in situ water vapour measurements were per-

formed both from balloon and sounding rocket and are based on OH fluorescence hygrometry (Kley and Stone, 1978; Khaplanov et al., 1992 and 1996). This fluorescence hygrometry technique employs active dissociation of water vapour at wavelengths below 137 nm by a vacuum ultraviolet (VUV) light source in order to produce electronically excited OH ($A^2\Sigma+$). This hydroxyl radical subsequently emits at wavelengths around 310 nm. From the intensity of this emission the actual water vapour concentration can be derived. Both the balloon and rocket instrument used a Lyman-α light source. The rocket light source had an about 20 times higher sensitivity as compared to the rocket light source used during Hygrosonde-1. This improvement was based on two major changes. First of all, instead of using only one discharge, the Hygrosonde-2 light source comprised six capillary discharges inside a single lamp body. On the other hand the lamp modulation, in order to discriminate the fluorescence signal from the background, was changed from a symmetrical to an asymmetrical cycle. This changed cycle employs shorter and stronger pulses and longer periods for the background determination. This measure significantly improved the signal-to-noise ratio. The measurements require an uncontaminated measurement volume. Hence, outgassing and desorption of water vapour from the payload itself are major challenges to the rocket-borne measurements. Even with highest precaution in the payload design outgassing and desorption cannot be completely avoided. Therefore, the key to undisturbed data is to perform the measurements outside the shock front, thus keeping contaminations due outgassing and desorption away from the measurement volume (Khaplanov et al., 1996). This aerodynamical concept is usually fulfilled on the ascent, so that the measurement technique is optimised for this part of the flight. On the descent, on the other hand, the measurements are usually influenced by contaminations. Useful data are only available from parts of the trajectory with aerodynamical favourable payload attitudes. The raw data are read out from the measurement every 2.5 ms. In order to increase the signal-to-noise ratio the raw data are then integrated over a period of 0.3 s. Hence the effective altitude resolution depends on the rocket velocity. At 40 km for example the effective altitude resolution is about 300 m, at 70 km the resolution is

CC BY

about 100 m better. The water vapour data from the balloon measurement are read out every second. No smoothing to these data has been applied. Assuming a typical balloon ascent rate of 5 ms^{-1} yields a vertical measurement resolution of 5 m.

The main Hygrosonde-2 rocket payload, carrying one of the hygrometers, was launched on 16 December 2001, 05:12 UT, reaching a top altitude of 90 km. This rocket carried also solid particle impact detectors from the University of Colorado (Horányi et al., 2000). For results from this experiment the reader is referred to Robertson et al. (2004). The Skerries balloon of the Swedish Institute for Space Physics in Kiruna was carrying the second hygrometer (Khaplanov et al., 2001). The balloon was launched at 04:58 UT and overlapped with the main rocket flight in time. It reached a top altitude of 25 km, providing also profiles of temperature, winds and density. Two meteorological rockets from NASA's Wallops Space Flight Center carrying falling spheres were launched right after the major Hygrosonde-2 rocket at 05:43 UT and 06:18 UT, respectively. These rocket measurements provided temperature, winds and density in the upper stratosphere and mesosphere (Schmidlin et al., 1991). The weather conditions (cloud cover) allowed only occasional measurements of the Rayleigh/Raman lidar of Bonn University (UBonn Lidar, Blum and Fricke, 2005) during the night. In total three hours of measurement were possible. These lidar measurements provided density and temperature profiles and monitoring of PSC presence. Complementary meteorological data have been obtained from the ECMWF.

3 Results

3.1 Local measurements

Figure 1 shows the combined water vapour profile measured during the Hygrosonde-2 campaign with the balloon and rocket-borne hygrometers. The balloon measurements (blue) covered the altitude range up to 25 km. Here, the data from the ascent of the balloon are shown. Water vapour measurements on the ascent rocket flight (green)

CC BY

were available above 45 km, after the opening of the nose cone of the rocket. The profile from the ascending flight could be used up to an altitude of 76 km for scientific analysis. Up to this altitude it could be assured that the measurements were made outside the shock front and were not influenced by contaminations from outgassing and desorption. The descending flight (red) provided data down to an altitude of 22 km. Contaminations from outgassing and desorption have been observed on the descent, as described in Sect. 2. These perturbed parts of the descent profile are not shown (gaps in the profile).

The water vapour concentration exhibit a sharp decrease in the upper troposphere and tropopause region. The hygropause is located at about 14 km, approximately 3 km above the tropopause, with a concentration of slight more than 4.0 ppmv. The water vapour volume mixing ratio increases strongly between 20 km and 30 km, from around 4 ppmv to more than 7 ppmv. A maximum can be observed at 32 km. Above 32 km the water vapour concentration decreases slightly with altitude, but recovers at an altitude of about 45 km. A second, but weaker, maximum can be observed at approximately 52 km. In a thin layer above, the water vapour concentration drops by around 1 ppmv, reaching a local minimum at an altitude of 55 km. At about 57 km a third distinct water vapour maximum is observable. Above 60 km the water vapour concentration decreases rapidly from more than 6 ppmv to around 2 ppmv at 70 km.

The measured profiles of the zonal (red) and meridional (blue) wind are plotted in Fig. 2. The lower part of the profiles is based on ascent data from the Skerries balloon, the upper part on the measurements by the second falling sphere. Wave structures, nearly in the entire altitude range covered by these measurements, clearly mark the influence by gravity waves. Most prominent is the strong wind shear in the altitude range between 60 km and 70 km.

The different temperature profiles measured by the balloon (blue), the second falling sphere (green) and the lidar instrument (red) are given in Fig. 3. The lidar measurement provided temperatures in the altitude range between 28 km and 54 km with a maximum error of 5 K. The tropopause is located at about 11 km altitude. The absolute minimum

CC BY

temperature is observed slightly below 25 km with somewhat less than 185 K. The low temperatures in this altitude region allow the formation and sustainment of PSC. The lidar measurements confirmed the presence of a PSC layer in this altitude region. The absolute maximum temperatures are observed at about 53 km and 60 km, at both altitudes the falling sphere measurements exhibit a temperature of 266 K. Like in the wind profiles clear signs of gravity wave activity can be observed in the temperature.

3.2 Polar vortex situation

During most of November 2001 the Arctic polar vortex has been strong and symmetrical in the stratosphere. On 30 November 2001 a minor warming occurred which disappeared on 8 December 2001. The vortex recovered in the following days until a very early major stratospheric warming occurred on 20 December 2001. This early warming was caused by the breaking of quasi-stationary waves (wave number 1) due to large-scale waves, which were propagating westward trough the stratosphere. These propagating waves had been initialized by strong tropospheric blockings which could be observed one to two weeks prior the warming (Naujokat et al., 2002).

The operational ECMWF data set for 6 UT on 16 December 2001 provides a nearly realtime overview of the polar vortex situation during the Hygrosonde-2 campaign. The ECMWF data shows a quite deformed and not at all circular shaped polar vortex below 530 K potential temperature (~23 km). In the altitude range between 530 K and 850 K potential temperature (~32 km) the ECMWF data shows a more pronounced polar vortex. Informations of the vortex situation at higher altitudes are not included operational ECMWF data set. Figure 4 shows the modified potential vorticity (Lait, 1993) field at the 850 K potential temperature level. As normalisation level the 475 K potential temperature level has been used. The two thick black contour lines describe the vortex edge region according to the criteria given by Nash et al. (1996). The vortex edge region is defined by the region between the local minimum and local maximum of the second derivative the potential vorticity around the mean polar vortex edge. The mean polar vortex edge itself is defined by the maximum gradient in the potential vorticity

ACPD
8, 12227–12252, 2008

constrained by the co-location of the maximum of the wind velocity. While the vortex edge is pronounced over Alaska, Siberia and northern Europe, it is somewhat disturbed over the Atlantic and Northern America. Here, non-vortex air could possibly enter the polar vortex area. Applying the criteria given by Nash et al. (1996) the location of the Esrange was outside the polar vortex below 530 K (~23 km) and inside between 530 K and 850 K potential temperature.

3.3 Gravity wave activity

The presence of gravity waves can clearly be seen in the local temperature and wind measurements. In order to determine the dominant waves we applied a hodograph analysis (e.g. Hirota and Niki, 1986) to the measured wind data. From the data we selected those altitude ranges where nearly monochromatic waves could be observed, namely 13.8 km to 17.5 km, 44.2 km to 47.7 km and 57.0 km to 67.6 km. The derived wave parameters in these three altitude ranges are summarised in Table 1. In all three altitude ranges selected, quasi-standing waves can be observed. The term "quasi" refers to the fact that we observe these waves only at single time and location and thus do not have any information about their time development. The clockwise rotation of the wind indicates upward propagating waves and energy, while the gravity wave phase moves downward. The waves observed in the lower and upper stratosphere have very similar characteristics in terms of vertical wavelength and intrinsic phase velocities. The wave in the mesosphere exhibits a somewhat different character with a much longer horizontal and vertical wavelength. The data do not contain any conclusive information about the excitation source of the observed waves. An excitation by the jet stream below the tropopause is not supported by the measured wind data since no pronounced jet can be observed. Likely these waves have been induced orographically by the Scandinavian mountain ridge which is the major excitation source in this area. The conditions for such excitation have been optimal between 9 December and 16 December 2001 without any exception. This can be concluded from the analysis of ECMWF data in accordance to criteria defined by Dörnbrack et al. (2001). Their criteria

ACPD
8, 12227–12252, 2008

are intended to determine the possibility of gravity wave excitation by the Scandinavian mountain ridge based on the horizontal wind velocity and its turning with altitude.

4 Discussion

The water vapour distribution observed during the Hygrosonde-2 campaign shows some very special characteristics, with respect to the general water vapour distribution described in the Sect. 1. The observations exhibit three distinct maxima in the water vapour concentration at about 32 km, 52 km and 57 km. We suggest that this aspect reflects measurements probing both vortex and extra-vortex air in different altitude ranges.

In the altitude range between 15 km and 19 km the observed water vapour concentration is rather constant with altitude. This consistency in the water vapour concentration indicates extra-vortex conditions. Typical water vapour concentrations outside the polar vortex are range between 4 ppmv and 5 ppmv in the altitude range between 16 km (~400 K potential temperature) and 26 km (~600 K) (e.g. de la Noë et al., 1999; Maturilli et al., 2006). From about 4.2 ppmv at 19 km altitude the water vapour concentration is increasing steadily to the first maximum at about 32 km, where a concentration of 7.7 ppmv can be observed. This strong increase in the lower and middle stratosphere is in general typical for the conditions inside the polar vortex (Maturilli et al., 2006). This conclusion is also supported by the analysis of the vortex edge location based on the criteria defined by Nash et al. (1996) using ECMWF operational data. According to that analysis a transition from the extra-vortex to the vortex should occur in the altitude range between 22 km (~500 K potential temperature) and 23 km (~530 K potential temperature) above the Esrange. The observed discrepany in the transition altitude between the in-situ measurements and the ECMWF model data is likely attributed to the rather coarse vertical and horizontal resolution of the ECMWF model in comparison to the smaller scale changes across the polar vortex edge. As a small scale deviation from the vortex inside picture drawn above, the observed water vapour

ACPD
8, 12227–12252, 2008

profile exhibits a small bite-out slightly below 22 km. The balloon measurement show a minimum concentration of about 4.6 ppmv in this very thin layer, which is characteristic for conditions outside the polar vortex as described above.

The observed maximum in the water vapour concentration at 32 km represents the conventional water vapour maximum for conditions inside the vortex, which is shifted downward due to the large scale subsidence of air inside the polar vortex. The observed altitude of the conventional maximum is somewhat lower than the examples found in the literature. Observations by ACE/FTS from 2004 show this water vapour peak slightly below 40 km altitude (Nassar et al., 2005). Aellig et al. (1996) report measurements with the Millimeter wave Atmospheric Sounder (MAS, Croskey et al., 1992) where they observed the maximum at about 1200 K potential temperature, which corresponds to an altitude of approximately 37 km. Results from the Polar Ozone and Aerosol Measurement (POAM) III instrument (Lucke et al., 1999) show occasionally a similar altitude of the conventional water maximum inside the polar vortex as our observation. In the average they find this maximum at an altitude of about 35 km in the Arctic winters between 1998/1999 and 2000/2001 (Nedoluha et al., 2002).

Up to an altitude of about 45 km the water vapour concentration decreases and the measurement has been performed inside the vortex. Above 45 km the water vapour concentration recovers, indicating that the measurement was made outside the polar vortex in this altitude range. At the transition altitude between vortex and extra-vortex at about 45 km also a nearly monochromatic gravity wave can be observed (see Table 1) which is likely involved in the advection of extra-vortex air. The second water vapour maximum at 51.5 km represents the conventional water vapour maximum for conditions outside the polar vortex. The maximum exhibits a concentration of 7.1 ppmv. This can be compared to typical water vapour concentrations inside the polar vortex that range between 3 ppmv and 5 ppmv in this altitude range, according to ACE/FTS observations (Nassar et al., 2005). A pronounced drop in the water vapour concentration above the second maximum results in a minimum at about 55 km. This minimum exhibits a water vapour concentration of 5.9 ppmv. Again, distinct gravity wave activity is evident in the

ACPD
8, 12227–12252, 2008

wind and temperature distribution in this altitude region. The observed water vapour concentration at this minimum is distinctly higher than those typical concentrations inside the polar vortex determined by ACE/FTS. This may indicate that only air from the edge between vortex and extra-vortex or the edge of a filament has been advected at this altitude. Higher up the water vapour concentration recovers and at 57 km a third distinct maximum (6.8 ppmv) in the observed water vapour distribution can be found. This third maximum is only part of the expected water vapour decrease above the extra-vortex conventional water vapour maximum around the stratopause. Then a sudden steep decrease of the water vapour concentration occurs around 60 km, connected to a gravity wave induced very strong wind shear. At 70 km a concentration of only 2 ppmv remains, a typical value for air from inside the polar vortex. Since the wind changed its direction from southwest to southeast, it can be concluded that vortex air was located southeast from the Esrange in this altitude range. Above 70 km the water vapour concentration recovers towards values which tend to be more representative for the extra-vortex, as observed by ACE/FTS.

The combination of the results from the Hygrosonde-2 campaign with the results from the Hygrosonde-1 campaign provides a very instructive and unique picture of the middle atmospheric water vapour distribution in the vicinity of the Arctic polar vortex. Figure 5 shows the water vapour profiles measured during both campaigns. The Hygrosonde-1 campaign consisted only of a single rocket flight carrying the hygrometer. The rocket was launched on 5 December 1994 at 00:50 UT from the Esrange and reached a top altitude of 77 km. The water vapour distribution could effectively be determined in the altitude range between 25 km and 68 km. Additional informations about the Hygrosonde-1 campaign can be found in Khaplanov et al. (1996). As evident from Fig. 5 the dynamical situation during Hygrosonde-1 was quite different in comparison to Hygrosonde-2. In contrast to the Hygrosonde-2 measurements which have been performed inside the polar vortex below 40 km the Hygrosonde-1 measurement probed extra-vortex air in this altitude range. This is also confirmed below 32 km by the analysis of the polar vortex edge location according to Nash et al. (1996), employing 40

year reanalysis data from ECMWF. At 32 km, the altitude where the conventional maximum inside the polar vortex could be observed during Hygrosonde-2, the difference in the water vapour concentration between the vortex and extra-vortex is about 3.6 ppmv. In comparison, the analysis of ACE/FTS measurements by Nassar et al. (2005) exhibits only a difference of less than 1 ppmv. In the entire altitude range above 45 km the Hygrosonde-1 water profile shows strong filament-like characteristics due to strong influence by gravity waves. This is consistent with the idea that the measurement took place at the very edge between vortex and extra-vortex in this altitude range. The gravity wave, with a vertical wavelength of 3 km to 5 km, causes the water vapour distribution to alternate between typical characteristics inside and outside the polar vortex. The water vapour contrasts between the vortex inside and outside suggested by the fluctuations in the Hygrosonde-1 profile are consistent with the vortex/extra-vortex contrasts suggested by Hygrosonde-2.

By comparing the water profiles from both Hygrosonde campaigns we can suggest representative profiles of the typical water vapour distribution inside and outside the Arctic polar vortex in the altitude range between 25 km and 70 km. These representative profiles are shown by the dashed lines in Fig. 5. As evident from the discussion of our results these typical distributions are in agreement with the ACE/FTS observations. Overall, the contrast between vortex and extra-vortex water vapour conditions is rather large. Furthermore our results provide additional evidence that the polar vortex still influences the horizontal mixing all the way up in the lower and middle mesosphere. In the altitude range between 60 km and 70 km the difference in the water vapour concentration between vortex and extra-vortex is more than 3 ppmv. Our results provide a valuable input for future modeling efforts. Current model results show a wide spread in the water vapour distribution in the polar vortex region. Furthermore the model calculations show in general not such distinct differences in the water vapour concentration between the vortex and extra-vortex (Eyring et al., 2006). These problems are basically due to an insufficient model resolution which in turn result in difficulties to resolve all wave effects.

5 Summary

The Hygrosonde-2 campaign has provided a detailed picture of the water vapour distribution in the vicinity of the polar vortex. Water vapour as a dynamical tracer has been used to determine the position of the measurement with respect to the polar vortex. This analysis showed that the Hygrosonde-2 profile has been measured inside the polar vortex in the middle stratosphere and middle mesosphere, while the measurement took place outside the polar vortex in the upper stratosphere and lower mesosphere. Transitions between vortex and extra-vortex usually coincided with wind shears caused by gravity waves. This observation reflects the role of gravity waves at the vortex edge, where they can advect air masses with different water vapour characteristics and thus influence the observed water profile.

From the results of the Hygrosonde-1 and Hygrosonde-2 campaign we derived typical water vapour profiles which represent the humidity structure inside and outside the polar vortex in the altitude range between 25 km and 70 km. The conventional water vapour maximum inside the polar vortex is located around 20 km lower as compared to extra-vortex. In general, the humidity contrasts between vortex and extra-vortex are rather large. The separating influence of the polar vortex on the water vapour distribution continues high up into the mesosphere. At altitudes as high as 70 km the polar vortex still prevents horizontal mixing of the different air masses, in agreement with the observations by ACE/FTS.

Acknowledgements. We thank the personnel of Swedish Space Corporation for their help during the Hygrosonde-2 campaign. This work was conducted with support from the Swedish National Space Board. We would like to acknowledge Farah Khosrawi for helpful comments on the manuscript.

References

Aellig, C. P., Bacmeister, J., Bevilacqua, R. M., Daehler, M., Kriebel, D., Pauls, T., Siskind, D., Kämpfer, N., Langen, J., Hartmann, G., Berg, A., Park, J. H., and Russell III, J. M.: Spaceborne H_2O observations in the Arctic stratosphere and mesosphere in the spring of 1992, Geophys. Res. Lett., 23, 2325–2328, 1996.

Bernath, P. F., McElroy, C. T., Abrams, M. C., Boone, C. D., Butler, M., Camy-Peyret, C., Carleer, M., Clerbaux, C., Coheur, P.-F., Colin, R., DeCola, P., DeMazière, M., Drummond, R., Dufour, D., Evans, W. F. J., Fast , H., Fussen, D., Gilbert, K., Jennings, D. E., Llewellyn, E. J., Lowe, R. P., Mahieu, E., McConnell, J. C., McHugh, M., McLeod, S. D., Michaud, R., Midwinter, C., Nassar, R., Nichitiu, F., Nowlan, C., Rinsland, C. P., Rochon, Y. J., Rowlands, N., Semeniuk, K., Simon, P., Skelton, R., Sloan, J. J., Soucy, M.-A., Strong, K., Tremblay, P., Turnbull, D., Walker, K. A., Walkty, I., Wardle, D. A., Wehrle, V., Zander, R., and Zou, J.: Atmospheric Chemistry Experiment (ACE): Mission overview, Geophys. Res. Lett., 32, L15S01, doi:10.1029/2005GL022386, 2005.

Blum, U. and Fricke, K. H.: The Bonn University lidar at the Esrange: Technical description and capabilities for atmospheric research, Ann. Geophys., 23(5), 1645–1658, 2005.

Bonazzola, M. and Haynes, P. H.: A trajectory-based study of the tropical tropopause region, J. Geophys. Res., 109, D20112, doi:10.1029/2003JD004356, 2004.

Brasseur, G. and Solomon, S.: Aeronomy of the middle atmosphere, D. Reidel Publishing Company, Dordrecht, 1984.

Brewer, A. W.: Evidence for a world circulation provided by the measurements of helium and water vapour distribution in the stratosphere, Q. J. Roy. Meteor. Soc., 75, 351–363, 1949.

Croskey, C. L., Kämpfer, N., Belivacqua, R. M., Hartmann, G. K., Kunzi, K. F., Schwartz, P. R., Olivero, J. J., Puliafito, S. E., Aellig, C., G., Umlauft, Waltman, W. B., and Degenhardt, W.: The Millimeter-Wave Atmospheric Sounder (MAS): A shuttle based remote sensing experiment, IEEE T. Microw. Theory, 40, 1090–1100, 1992.

de la Noë, J., Ovarlez, J., Ovarlez, H., Schiller, C., Lautié, N., Ricaud, P., Urban, J., Feist, D. G., Zalesak, L., Kämpfer, N., Ridal, M., Murtagh, D., Lindner, K., Klein, U., Künzi, K., Forkman, P., Winnberg, A., Hartogh, P., and Engel, A.: Water vapour distribution inside and outside the polar vortex during THESEO, Fifth European Symposium on Stratospheric Ozone, St. Jean de Luz/France, Pollution Research Report, edited by: Harries, N. R. P., Guirlet, M., and Amanatidis, G. T., 73, 558–561, 2000.

Dörnbrack, A., Leutbecher, M., Reichardt, J., Behrendt, A., Müller, K.-P., and Baumgarten, G.: Relevance of mountain wave cooling for the formation of polar stratospheric clouds over Scandinavia: Mesoscale dynamics and observations for January 1997: J. Geophys. Res., 106(D2), 1569–1582, doi:10.1029/2000JD900194, 2001.

Engel, A., Bönisch, H., Brunner, D., Fischer, H., Franke, H., Günther, G., Gurk, C., Hegglin, M., Hoor, P., Königstedt, R., Krebsbach, M., Maser, R., Parchatka, U., Peter, T., Schell, D., Schiller, C., Schmidt, U., Spelten, N., Szabo, T., Weers, U., Wernli, H., Wetter, T., and Wirth, V.: Highly resolved observations of trace gases in the lowermost stratosphere and upper troposphere from the Spurt project: an overview, Atmos. Chem. Phys., 6(2), 283–301, 2006.

Eyring, V., Butchart, N., Waugh, D. W., Akiyoshi, H., Austin, J., Bekki, S., Bodeker, G. E., Boville, B. A., Brühl, C., Chipperfield, M. P., Cordero, E., Dameris, M., Deushi, M., Fioletov, V. E., Frith, S. M., Garcia, R. R., Gettelman, A., Giorgetta, M. A., Grewe, V., Jourdain, L., Kinnison, D. E., Mancini, E., Manzini, E., Marchand, M., Marsh, D. R., Nagashima, T., Newman, P. A., Nielsen, J. E., Pawson, S., Pitari, G., Plummer, D. A., Rozanov, E., Schraner, M., Shepherd, T. G., Shibata, K., Stolarski, R. S., Struthers, H., Tian, W., and Yoshiki, M.: Assessment of temperature, trace species, and ozone in chemistry-climate model simulations of the recent past, J. Geophys. Res., 111, D22308, doi:10.1029/2006JD007327, 2006.

Hirota, I. and Niki,T.: Inertia-gravity waves in the troposphere and stratosphere observed by the MU radar, Meteorological Society of Japan; 64, 995–999, 1986.

Horányi, M., Robertson, S., Smiley, B., Gumbel, J., Witt, G., and Walch, B.: Rocket-borne mesospheric measurement of heavy charge carriers, Geophys. Res. Lett., 27, 3825–3828, 2000.

Kelly, K. K., Tuck, A. F., Murphy, D. M., Proffitt, M. H., Fahey, D. W., Jones, R. L., McKenna, D. S., Loewenstein, M., Podolske, J. R., Strahan, S. E., Ferry, G. V., Chan, K. R., Vedder, J. F., Gregory, G. L., Hypes, W. D., McCormick, M. P., Browell, E. V., and Heidt, L. E.: Dehydration in the lower Antarctic stratosphere during late winter and early spring 1987, J. Geophys. Res., 94, 11 317–11 357, 1989.

Khaplanov, M., Astakhov, V., Lukjanov, A., Kretova, M., and Yushkov, V.: Fluorescent hygrometer for middle atmosphere measurements; Proceedings of the 19th Annual European Meeting on Atmospheric Studies by Optical Methods, 540–545, 1992.

Khaplanov, M., Gumbel, J., Wilhelm, N., and Witt, G.: Hygrosonde – A direct measurement of water vapour in the stratosphere and mesosphere, Geophys. Res. Lett., 23, 1645–1648,

1996.
Khaplanov, M., Gumbel, J., Witt, G., and Kirkwood, S.: Studies of troposphere/stratosphere humidity structures during the Skerries balloon programme, Proceedings of the 15th ESA Symposium on European Rocket and Balloon Programmes and Related Research (ESA SP-471), 283–286, 2001.
Kley, D. and Stone, E. J.: Measurement of water vapour in the stratosphere by photodissociation with Ly α(1216°) light, Rev. Sci. Instrum., 49, 691–697, 1978.
Lait, L. R.: An alternative form for potential vorticity; J. Atmos. Sci., 51(12), 1754–1759, 1993.
Lelieveld, J., Brühl, C., Jöckel, P., Steil, B., Crutzen, P. J., Fischer, H., Giorgetta, M. A., Hoor, P., Lawrence, M. G., Sausen, R., and Tost, H.: Stratospheric dryness: model simulations and satellite observations, Atmos. Chem. Phys., 7(5), 1313–1332, 2007.
Lucke, R. L., Korwan, D. R., Bevilacqua, R. M., Hornstein, J. S., Shettle, E. P., Chen, D. T., Daehler, M., Lumpe, J. D., Fromm, M. D., Debrestian, D., Neff, B., Squire, M., König-Langlo, G., and Davies, J.: The Polar Ozone and Aerosol Measurement (POAM) III instrument and early validation results, J. Geophys. Res., 104(D15), 18 785–18 799, 1999.
M. Maturilli, Fierli, F., Yushkov, V., Lukyanov, A., Khaykin, S., and Hauchecorne, A.: Stratospheric water vapour in the vicinity of the Arctic polar vortex, Ann. Geophys., 24, 1511–1521, 2006, http://www.ann-geophys.net/24/1511/2006/.
Michelsen, H. A., Irion, F. W., Manney, G. L., Toon, G. C., and Gunson, M. R.: Features and trends in Atmospheric Trace Molecule Spectroscopy (ATMOS) version 3 stratospheric water vapor and methane measurements, J. Geophys. Res., 105(D18), 22 713–22 724, 2000.
Mote, P. W., Rosenlof, K. H., McIntyre, M. E., Carr, E. S., Gille, J. C., Holton, J. R., Kinnersley, J. S., Pumphrey, H. C., Russell III, J. M., and Waters, J. W.: An atmospheric tape recorder: The imprint of tropical tropopause temperatures on stratospheric water vapor, J. Geophys. Res., 101(D2), 3989–4006, 1996.
Naujokat, B., Krüger, K., Matthes, K., Hoffmann, J., Kunze, M., and Labitzke, K.: The early major warming in December 2001 – exceptional?, Geophys. Res. Lett., 29(21), 2023, doi:10.1029/2002GL015316, 2002.
Nash, E. R., Newman, P. A., Rosenfield, J. E., and Schoeberl, M. R.: An objective determination of the polar vortex using Ertel's potential vorticity, J. Geophys. Res., 101(D5), 9471–9478, 1996.
Nassar, R., Bernath, P. F., Boone, C. D., Manney, G. L., McLeod, S. D., Rinsland, C. P., Skelton,

R. S., and Walker, K. A.: ACE-FTS measurements across the edge of the winter 2004 Arctic vortex, Geophys. Res. Lett., 32, L15S05, doi:10.1029/2005GL022671, 2005.
Nedoluha, G. E., Bevilacqua, R. M., Gomez, R. M., Waltman, W .B., Hicks, B. C., Thacker, D. L., and Matthews, W. A.: Measurements of water vapor in the middle atmosphere and implications for mesospheric transport, J. Geophys. Res., 101(D16), 21 183–21 194, doi:10.1029/96JD01741, 1996.
Nedoluha, G. E., Bevilacqua, R. M., and Hoppel, K. W.: POAM III measurements of dehydration in the Antarctic and comparisons with the Arctic, J. Geophys. Res., 107(D20), 8290, doi:10.1029/2001JD001184, 2002.
Nedoluha, G. E., Bevilacqua, R. M., Gomez, R. M., Hicks, B. C., Russell III J. M., and Connor, B. J.: An evaluation of trends in middle atmospheric water vapor as measured by HALOE, WVMS, and POAM, J. Geophys. Res., 108(D13), 4391, doi:10.1029/2002JD003332, 2003.
Oltmans, S. J., Vömel, H., Hofmann, D. J., Rosenlof, K. H., and Kley, D.: The increase in stratospheric water vapor from balloon-borne, frostpoint hygrometer measurements at Washington, D.C. and Boulder, Colorado, Geophys. Res. Lett., 27(21), 3453–3456 2000.
Randel, W. J., Wu, F., Oltmans, S. J., Rosenlof, K. H., and Nedoluha, G. E.: Interannual changes of stratospheric water vapor and correlations with tropical tropopause temperatures; J. Atmos. Sci., 61(17), 2133–2148, 2004.
Reid, S. J. and Vaughan, G.: Lamination in ozone profiles in the lower stratosphere, Q. J. Roy. Meteor. Soc., 117, 825–844, 1991.
Rex, M., Salawitch, R. J., von der Gathen, P., Harris, N. R. P., Chipperfield, P., and Naujokat, B.: Arctic ozone loss and climate change; Geophys. Res. Lett., 31, L04116, doi:10.1029/2003GL018844, 2004.
Robertson, S., Horanyi, M., and Sternovsky, Z.: Rocket-borne probes for charged mesospheric aerosol particles, Proceedings of 35th COSPAR Scientific Assembly, Paris/France, 1887, 2004.
Rosenlof, K. H., Chiou, E.-W., Chu, W. P., Johnson, D. G., Kelly, K. K., Michelsen, H. A., Nedoluha, G. E., Remsberg, E. E., Toon, G. C., and McCormick,M. P.: Stratospheric water vapor increases over the past half-century, Geophys. Res. Lett., 28(7), 1195–1198, 2001.
Schmidlin, F. J., Lee, H. S., and Michel, W.: The inflatable sphere: A technique for the accurate measurements of middle atmospheric temperatures, J. Geophys. Res., 96, 22 673–22 682, 1991.
Seele, C. and Hartogh, P.: Water vapour of the polar middle atmosphere: Annual variation

and summer mesosphere conditions as observed by ground-based microwave spectroscopy, Geophys. Res. Lett., 25, 2133–2136, 1999.

Sherwood, S. C. and Dessler, A. E.: On the control of stratospheric humidity, Geophys. Res. Lett., 27, 2513–2516, 2000.

Sonnemann, G. R., Grygalashvyly, M., and Berger, U.: Autocatalytic water vapor production as a source of large mixing ratios within the middle to upper mesosphere, J. Geophys. Res., 110, D15303, doi:10.1029/2004JD005593, 2005.

Stratospheric Processes and Their Role in Climate (SPARC), SPARC Assessment of upper tropospheric and stratospheric water vapour, edited by: Kley, D., Russell III, J. M., and Philips, C., WMO/ICSU/IOC World Climate Research Programme, Geneva, 2000.

Summers, M. E., Conway, R. R., Siskind, D. E., Stevens, M. H., Offermann, D., Riese, M., Preusse, P., Strobel, D. F., and Russell III, J. M.: Implications of satellite OH observations for middle atmospheric H_2O and ozone Science, 277, 1967–1970, 1997.

Summers, M. E., Conway, R. R., Englert, C. R., Siskind, D. E., Stevens, M. H., Russell III, J. M., Gordley, L. L., and McHugh, M. J.: Discovery of a water vapor layer in the Arctic summer mesosphere: Implications for polar mesospheric clouds, Geophys. Res. Lett., 28(18), 3601–3604, 2001.

von Zahn, U. and Berger, U.: Persistent ice cloud in the midsummer upper mesosphere at high latitudes, Three-dimensional modeling and cloud interactions with ambient water vapour, J. Geophys. Res., 108(D7), 8451, doi:10.1029/2002JD002409, 2003.

Vömel, H., Oltmans, S. J., Hofmann, D. J., Deshler, T., and Rosen, J. M.: The evolution of the dehydration in the Antarctic stratospheric vortex, J. Geophys. Res., 100, 13 919–13 926, 1995.

Table 1. Overview of the dominating gravity waves determined by the hodograph analysis in three selected altitude ranges.

Altitude range [km]	13.8–17.5	44.2–47.7	57.0–67.6
Period [h]	6,9	5,7	8,2
Horizontal wavelength [km]	370	261	1100
Vertical wavelength [km]	3,7	3,5	10,6
Intrinsic horizontal phase velocity [m/s]	15	13	38
Intrinsic vertical phase velocity [m/s]	–0,15	– 0,17	–0,36

ACPD

8, 12227–12252, 2008

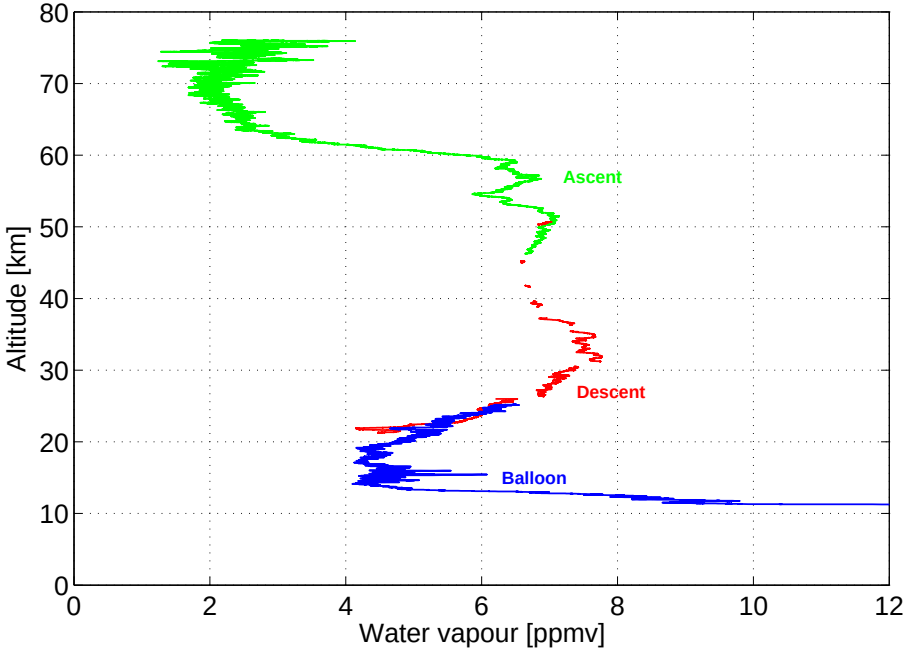

Fig. 1. The water vapour profile derived from the OH flourescence hygrometer measurements onboard the Skerries balloon (ascent) and the rocket (ascent and descent).

ACPD
8, 12227–12252, 2008

Title Page
Abstract Introduction
Conclusions References
Tables Figures
◀I ▶I
◀ ▶
Back Close
Full Screen / Esc
Printer-friendly Version
Interactive Discussion

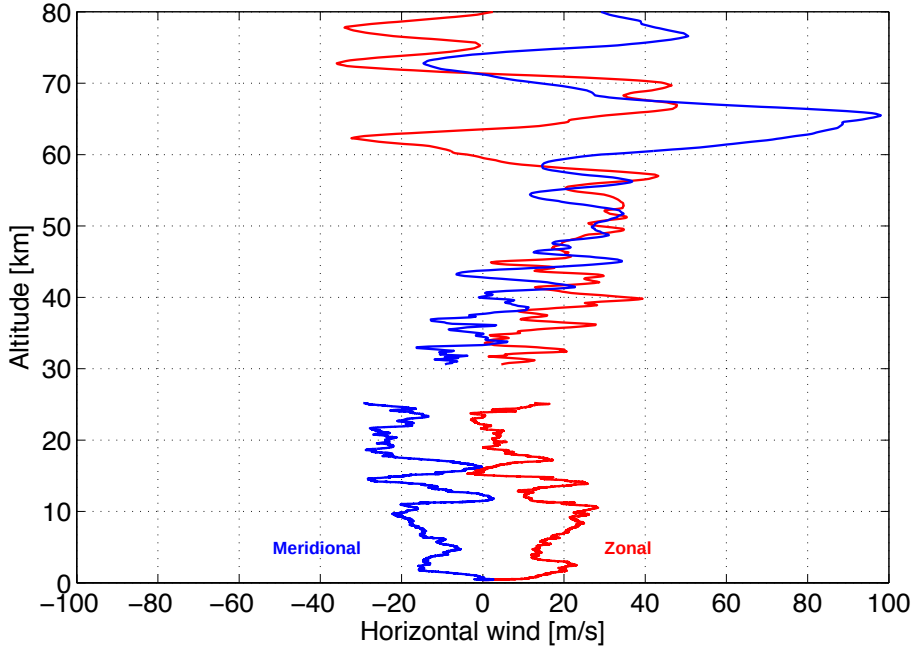

Fig. 2. Zonal and meridional winds measured by the Skerries balloon (below 25 km) and the second falling sphere (above 33 km).

ACPD
8, 12227–12252, 2008

Title Page
Abstract Introduction
Conclusions References
Tables Figures
◀I ▶I
◀ ▶
Back Close
Full Screen / Esc
Printer-friendly Version
Interactive Discussion

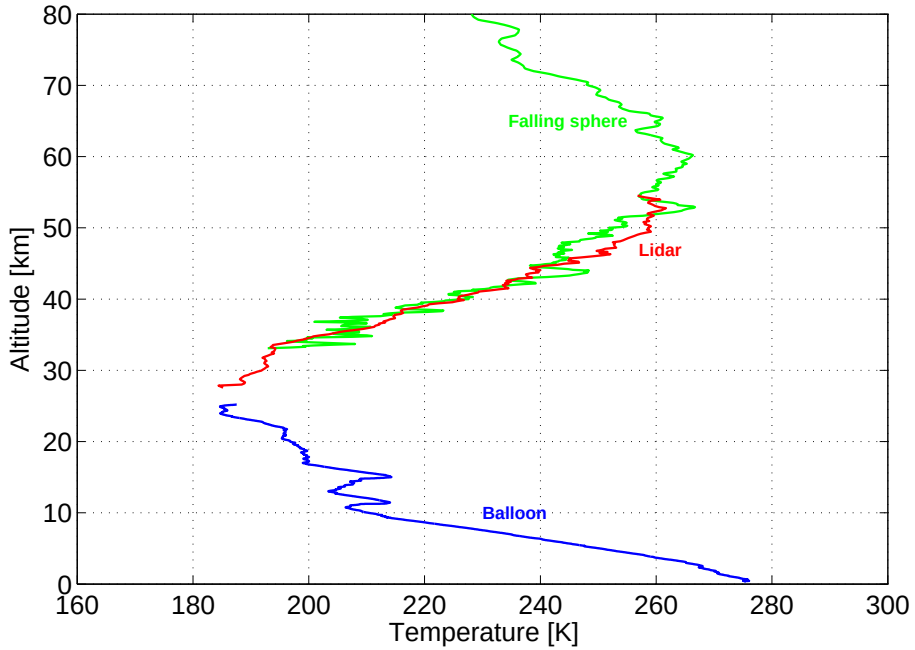

Fig. 3. Temperature profile derived from falling sphere, lidar and balloon measurements.

ACPD
8, 12227–12252, 2008

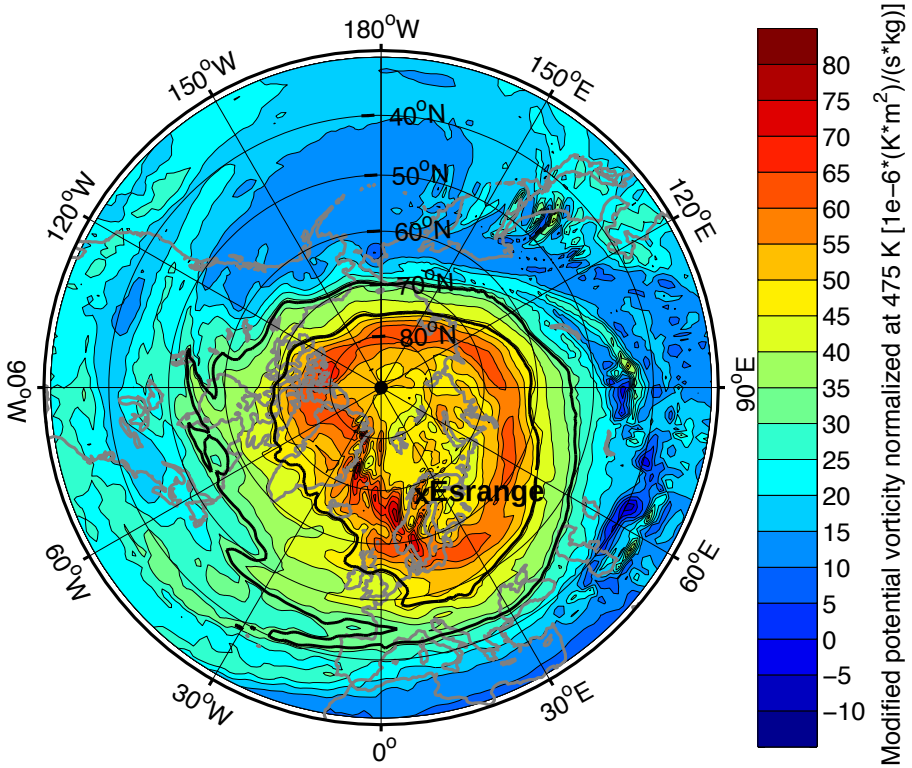

Fig. 4. The distribution of the modified potential vorticity at the 850 K potential temperature level (~32 km). The normalisation level has been 475 K. The two thick contour lines mark the polar vortex boundary region according to the criterion defined by Nash et al. (1996).

ACPD
8, 12227–12252, 2008

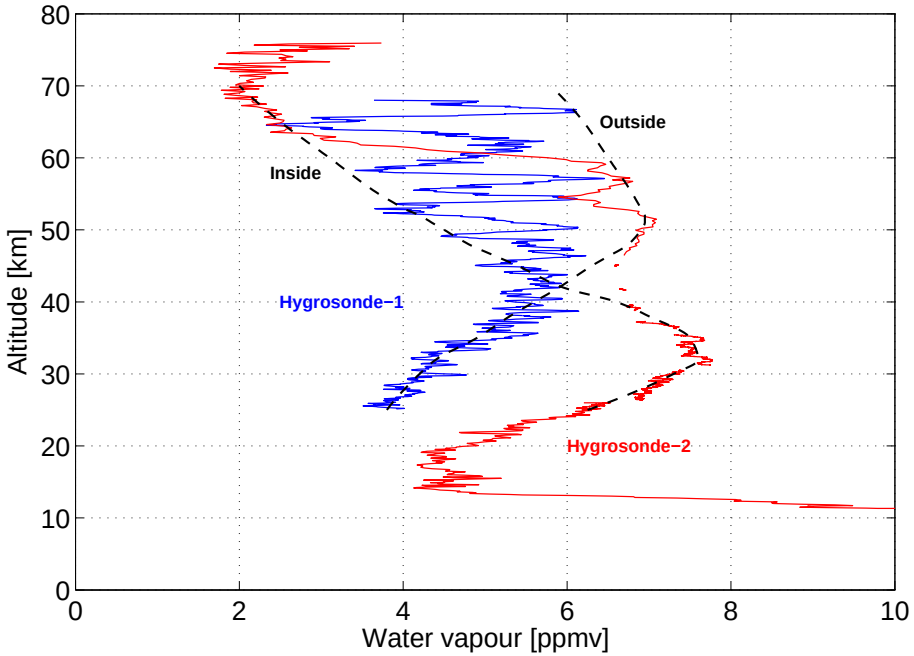

Fig. 5. The water vapour profiles measured during the Hygrosonde-1 and Hygrosonde-2 campaign. The dashed lines represent typical water distributions inside and outside the polar vortex that are consistent with the measurements from these two campaigns.

ACPD
8, 12227–12252, 2008